1

INTRODUCTION

1

THE amount of data that is globally being created, processed, and stored is increasing at a remarkable pace. Furthermore, the advent of new technologies, such as augmented reality (AR), autonomous driving, computer vision, and many other emerging techniques, requires on-the-fly processing of large data files, such as images, at an increasing rate. Image processing is usually performed digitally but the speed and power consumption limits of standard microelectronic components have become a true bottleneck. Analog optical processing provides a promising route that may overcome these limitations. Also, processing signals in the optical domain enables massive parallelization and may potentially avoid unnecessary analog-to-digital conversion.

While a lot of data is nowadays stored, guided, and routed in the optical domain, computing is still mainly performed digitally. The idea of computing optically can be traced back to the early 1960s prompted by pioneering work that ingeniously exploited concepts of Fourier optics [1–4]. Among others, all-optical pattern recognition and optical processing of synthetic–aperture radar (SAR) data were the most successful. The freedom of choice about the linear transformation allowed by a generic spatial filter prompted the idea of designing responses in k–space specific to a certain type of input. This is the concept at the base of matched spatial filters and, in turn, at the core of optical pattern recognition [5–8]. As shown in Figure 1.1a, an optical processor is able to discriminate the character contained in the input image and signals the answer with a bright spot under the letter "P". More elaborate approaches even achieved real–time face recognition [9].

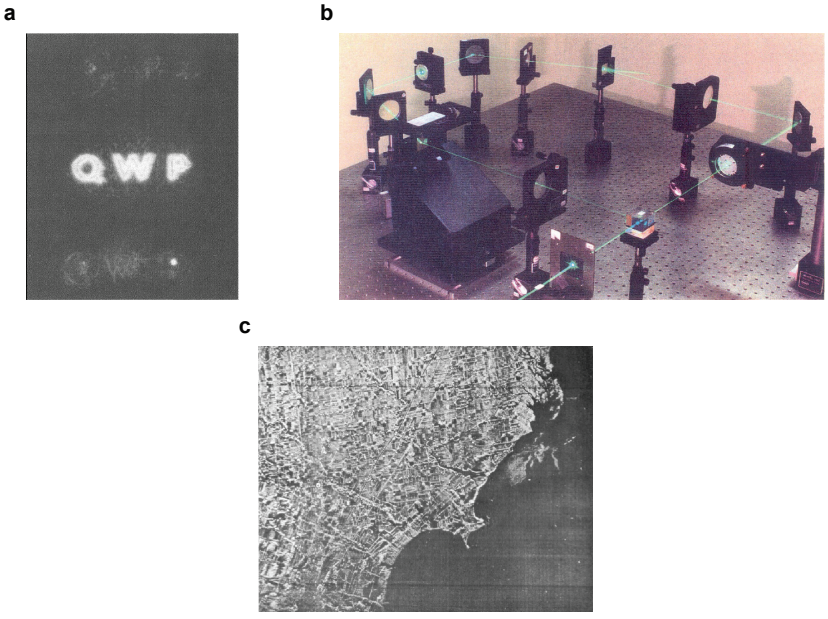

Figure 1.1: **a** A set of matched spatial filters can recognize an input character. The bright spot signals the outcome of the recognition scheme [10]. **b** Photograph of a pattern–recognition system [4]. **c** Synthetic–aperture radar image of Monroe, MI (USA) [2].

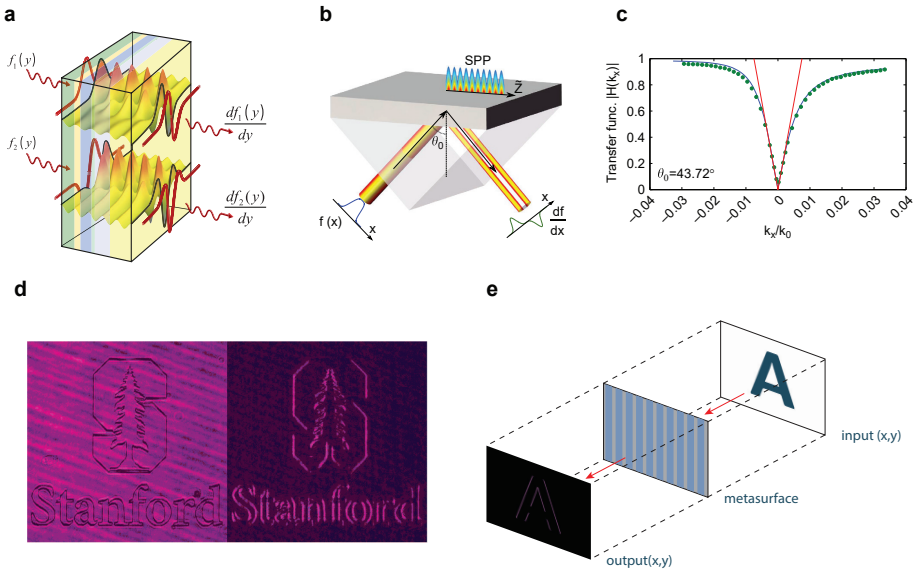

Figure 1.2: **a** Conceptual sketch of a GRIN–based metamaterial performing 1st– or 2nd–order derivative. Re-adapted from Ref. [11]. **b** Plasmonic spatial differentiator exploiting SPP. **c** Spatial transfer function spectra of the sample sketched in b, experimental measurement (dotted lines) and numerical fitting (solid lines). **d** Input image modulated in phase and output image demonstrating edge detection. Panels b-d re-adapted from Ref. [14]. **e** Schematics of a metasurface performing edge filtering in transmission [19].

Optical processors based on Fourier optics were also successfully used to apply linear transformations on data sets that are not human-readable. Specifically, in the mid-1960s, Cutrona et al. [2] found a way to convert the microwave reflectivity signals acquired by special side–looking airplane radars (SARs) into high–resolution pictures (see Figure 1.1c). These elegant all-optical solutions, however, require bulky optical components that are not integrable into nanophotonic or microelectronic systems; hence, as the transistor size scaled-down dramatically and digital computational power skyrocketed, these approaches became quickly obsolete.

The unprecedented control of light propagation over a sub-wavelength thickness that has been recently enabled by optical metasurfaces opens entirely new opportunities for analog optical computing [11–19]. In fact, "computing metasurfaces" may benefit from the speed and low power consumption of optics while being amenable to on-chip integration, thus enabling hybrid optical and electronic data processing on a single chip.

In this context, the work of Silva et al. [11] is groundbreaking as it introduced the idea of using suitably designed metamaterials to perform arbitrary mathematical operations. As conceptually illustrated in Figure 1.2a, a series of optimized graded–index (GRIN) dielectric slabs can transform a given input wave signal $f(y)$ into its 1st– or 2nd–order derivative. Despite the high conceptual impact, this approach remained experimentally unpractical given the complexity of the design.

More recently, a simpler approach based on plasmonic resonances [14] demonstrated

experimentally all-optical edge detection. This work exploits the possibility of coupling to Surface Plasmon Polaritons (SPP) at the interface between air and metal by means of a prism (Kretschmann configuration) [20]. Indeed, for a given metal thickness, light is efficiently coupled only at a specific angle due to momentum matching while the metal surface is completely reflective when this condition is not met. This, in turn, results in a sharp dip in the transfer function of the system which can be used efficiently as a high pass filter (see Figure 1.2b-d): the edges of an input image (Stanford tree logo) modulated in phase are enhanced in the output image as a result of the spatial filtering. The drawbacks of this configuration are the limited numerical aperture (NA) and the use of bulky elements: while the former (NA~ 0.01) implies low spatial resolution and does not allow readily integration in imaging systems (which usually have larger NA), the latter further hinders on-chip implementation.

Sparked by these and other pioneering works, the possibility of shaping the spatial content of an image by suitably engineering a structure's response in k–space prompted a multitude of interesting studies [21–23]. These, either exploit resonant effects of different nature induced by nanopatterns or are based on planar stacks of different materials or even single interfaces. In the latter category, as an example, the well known Brewster effect, where TM-polarized light is not reflected off a single interface at a specific angle, has been exploited to create a zero in the transfer function and thus perform optical differentiation [24]. Similarly, other studies utilize effects observed when an incident polarized beam reflected from a flat surface is subsequently analyzed with a polarizer [25–28]. In this configuration, Zhu et al. [28] established a connection between two-dimensional optical spatial differentiation and a nontrivial topological charge in the optical transfer function. Similar to the example described in Figure 1.2b-d, these elegant solutions are very insightful and further deepen the understanding of analog image processing. Nevertheless, these examples are impractical from an application point of view.

While more difficult to fabricate, spatial differentiators based on thin nanopatterned surfaces (see Figure 1.2e) are more flexible in terms of transfer function design and more applicable to real imaging devices. In theoretical studies, Guo et al. [17, 18] designed photonic crystal slab spatial filters by engineering the photonic band structure, and related guided-mode resonances, to be isotropic at the Γ-point. Using this rationale, they proposed two different structures capable of performing the Laplacian operator [17] and isotropic high-pass, low-pass, band-reject, and band-pass filtering [18]. However, also in these cases the NA~ 0.01. Following up, Zhou et al. [29] realized experimentally a quasi-isotropic second order differentiator based on a Si metasurface. Moreover, the latter was coupled to a metalens obtaining a monolithic compound flat optical elements. Whereas the possibility of vertically stacking metasurfaces opens new exciting prospects also for the design of more complex mathematical operations, this specific combination (metalens and metasurface-based differentiator) does not really translate into a dramatically more compact optical device. The footprint of this monolithic image-processing system remains constrained by the focal distance between the metalens and the imaging camera.

Interestingly, also in this context, structures with judiciously optimized k-space response can be exploited to miniaturize optical systems by "compressing" the free space in between the components [30, 31]. To achieve this, one has to engineer metasurfaces

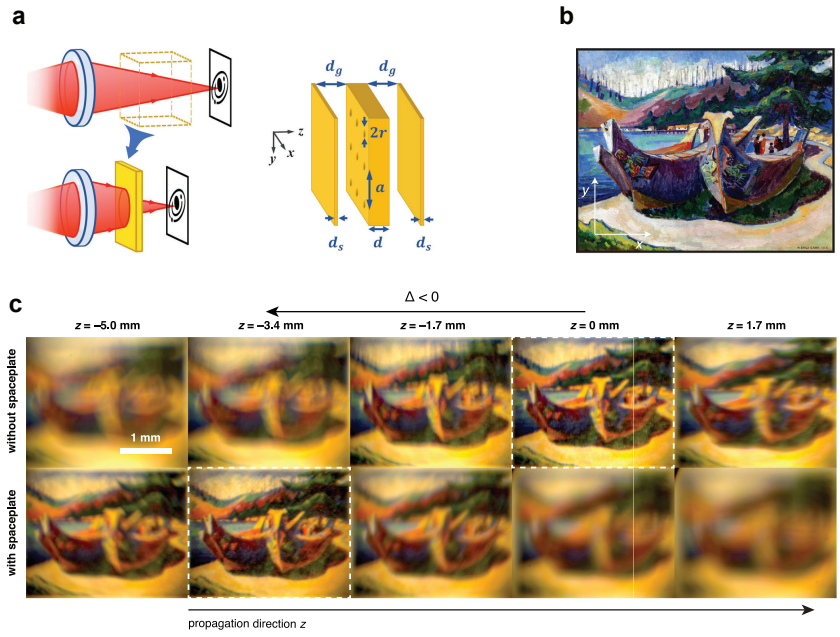

Figure 1.3: **a** Schematics showing a general optical system and the concept of free-space compression. The free-space in the yellow dashed box can be replaced by a smarty designed photonic crystal slab. Re-adapted from Ref. [30]. **b** Painting illuminated with incoherent white light used as image object. **c** The image of the print is formed in either a background medium (glycerol), or through the calcite spaceplate in glycerol. Camera images at various distances z. The spaceplate advances the focal plane of the image by −3.4 mm relative to the glycerol alone. Panels b-c re-adapted from Ref. [31].

with a physical thickness t having the transfer function corresponding to free space propagation over a distance $d > t$. The ratio d/t can be thought of as a compression factor. The transfer function of free space imparts the appropriate phase lag to each plane wave constituting the spatial content of an image without altering the amplitude. Figure 1.3a illustrates schematically how a portion of free space (yellow dashed box) can be substituted by a properly designed photonic crystal slab design [30]. Almost at the same time, Reshef et al. [31] proposed metamaterial "spaceplates" composed of alternating layers of Si and SiO_2 with compression factors up to ~ 4.9. Moreover, they experimentally demonstrated free space compression with a bulk calcite sample. Using a standard imaging system, a 3.4 mm shift in the optimal focus distance was observed (see Figure 1.3b-c). It is worth noting that the spaceplate does not change the magnification.

The concept of optical analog computing goes beyond image processing and filtering. Indeed, fueled by the recent advances in inverse design algorithms [32–37], the group of Engheta demonstrated a metamaterial platform that can solve integral equations in an analog fashion [38]. Specifically, an arbitrary input function is encoded into wave signals that are sent to the structure in Figure 1.4a and are transformed into the integral of the input upon interaction with the metamaterial. The latter is governed by

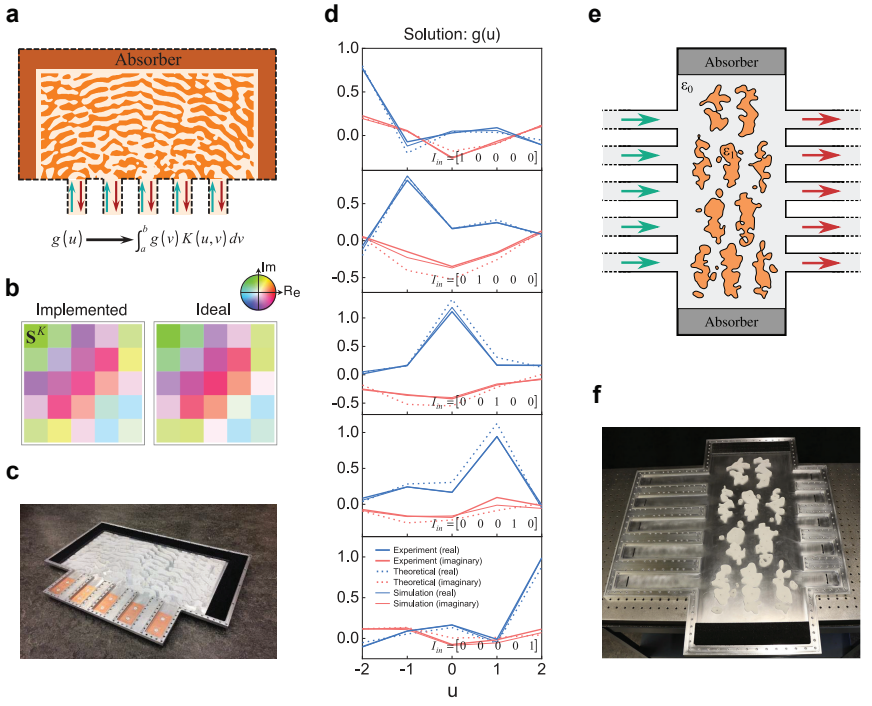

Figure 1.4: **a** Schematics of the analog integral solver in a reflective set-up, consisting of the inverse designed metamaterial kernel and in/out coupling elements to excite and probe the waves. **b** Comparison between the implemented and the desired kernel operator. **c** Photograph of the constructed metamaterial structure. The device width ~ 66 cm. **d** Experimentally measured output signals as the solutions to the integral equation with kernel in panel b. Measurements are compared with the expected theoretical results (dashed lines) and full-wave simulations (thin lines), for applied input signals at each of the five ports (one by one). Panels a-d re-adapted from Ref. [38]. **e** Inverse-designed dielectric distribution that reproduces the two desired mathematical kernels when two waves with two frequencies ω_1 and ω_2 are used. **f** Photograph of the constructed device. Panels e-f re-adapted from Ref. [39].

the scattering matrix of the metastructure that acts as the kernel of the integral operator. Such scattering matrix can be designed at will via inverse design, as shown in Figure 1.4b. Next, by repeatedly returning the signal to the structure with a feedback loop the input function rapidly converges to the solution of the integrals equation associated with the designed kernel.

This approach was experimentally demonstrated at microwave frequencies proving the solution of a generic integral equation. Figure 1.4d highlights the comparison between the experimentally measured output signals (in real and imaginary part) and the theoretical solution to the integral equation featuring the desired kernel in Figure 1.4b for applied input signals at each of the five ports. In a follow-up study [39] the same group investigated and experimentally fabricated a single metastructure that simultaneously solves different integral equations at different frequencies in a parallel way (see

Figure 1.4e-f). It is worth highlighting that, the two devices showcased can also be used to invert arbitrary matrices by suitably designing the kernel. Finally, the main limitation of such analog implementations in the microwave frequency range is the meter-scale device footprint.

MOTIVATION AND OUTLINE OF THE THESIS

The ever-growing need for efficient computing has been driving researchers from diverse research fields to explore alternatives to the current digital computing paradigm. As mentioned, the processing speed and energy efficiency of standard electronics have become limiting factors for novel disruptive applications entering our everyday life, such as artificial intelligence, machine learning, computer vision, and many more.

In this context, analog computing has resurfaced and regained significant attention as a complementary route to traditional architectures. Specifically, the tremendous recent advances in the field of metamaterials and metasurfaces have been unlocking new opportunities for all-optical computing strategies, given the possibility of shaping optical fields in extreme ways over sub-wavelength thicknesses. The absence of bulky optical elements, in turn, enables on-chip integration.

In this thesis, we introduce different metasurface-based platforms that perform image processing tasks or solve complex mathematical problems within a form factor that remains on-chip amenable. In fact, all-optical processing is not meant to replace digital computing but rather to ease its burden, paving the way for hybrid optical and electronic data processing. To achieve this, we design and demonstrate experimentally for the first time all-optical processing metasurfaces that are sub-wavelength in thickness and work in transmission with significantly larger and practical NA, further facilitating application into standard imaging systems (e.g. smartphone cameras). Furthermore, we explore the possibility of tuning the operation imparted on an input signal in a CMOS compatible configuration. Finally, we apply the concept of a wave base integral solver to the optical wavelength range. This, in turn, implies a drastic footprint reduction and thus, again, makes the device on-chip amenable. Moreover, smaller size results in an increased processing speed as light has to travel shorter distances.

In **Chapter 2**, we introduce dielectric metasurfaces that perform optical image edge detection in the analog domain using a sub–wavelength geometry that can be readily integrated with detectors. The metasurface is composed of a suitably engineered array of nanobeams designed to perform either 1^{st}– or 2^{nd}–order spatial differentiation in the visible spectral range. We present a design recipe to tailor the spatial dispersion of the metasurface by introducing a Fano resonance in transmission and the resulting optimized transfer functions are tested numerically demonstrating close-to-ideal performances. Next, the fabrication process is described step by step both for the metasurface and for the images that are used as diapositives. We experimentally demonstrate the 2^{nd}–derivative operation on input images, showing the potential of all-optical edge detection using a silicon metasurface geometry working at a practically relevant numerical aperture as large as 0.35. Finally, we extend the formalism used to 2D operations and unpolarized illumination. Optimized designs performing quasi-isotropic even– and odd–order spatial differentiation are presented and demonstrate numerically edge detection in all directions. Appendix A contains the calculations supporting Chapter 2,

including the coupled–mode theory derivation needed in the design section.

Chapter 3 describes the first proof-of-concept of an electrically controllable metasurface for optical processing. To achieve this, a metasurface sustaining a Fano resonance is coupled to an electrically gated WS_2 monolayer. The suppression of the excitonic resonance in the quasi-two-dimensional material has a big impact on its optical response and thus alters the metasurface transfer function. This rationale is used to design a switchable Fourier spatial filter. Specifically, the device acts as a high-pass filter that can be perturbed by the presence (or absence) of excitons in the WS_2 monolayer. Numerical tests on an optimized design clearly demonstrate reliable edge filtering that can be turned on and off at specific illumination wavelengths. Next, a chip containing several devices is realized and the fabrication steps are discussed in detail. Optical characterization under an applied external bias shows a small modulation of the Fano resonance in reflectance following the same trends of the simulations, showing the potential of the proposed hybrid metasurface–2D-TMD platform. The results shown in the chapter are the first step for optical computing metasurfaces devices with functionalities that can be tuned during operation.

Within **Chapter 4**, we present an ultra-thin Si metasurface-based platform for analog computing that is able to solve Fredholm integral equations of the second kind using free-space visible radiation. A Si-based metagrating is inverse-designed to implement the scattering matrix synthesizing a prescribed Kernel corresponding to the mathematical problem of interest. Next, a semi-transparent mirror is incorporated into the sample to provide adequate feedback and thus perform the required Neumann series solving the corresponding equation in the analog domain at the speed of light. The solution provided by the metasurface in simulation effectively solves the problem of interest and is very close to its ideal counterpart. Electron beam lithography and reactive ion etching provide the resolution required to create a hardware representation of a predefined kernel, with relatively small deviations between experiment and simulations. We optically characterize the output for different input signals showing good agreement with the ideal simulated response and we use the spectral data to retrieve the experimental solution again showing good agreement with theory. Visible wavelength operation enables a highly compact, ultra-thin device that can be interrogated from free-space, implying high processing speeds and the possibility of on-chip integration.

Finally, in **Chapter 5** we apply the gained knowledge about gratings to a completely different task. The results presented in this chapter demonstrate a nanophotonic light trapping scheme aimed at boosting the efficiency of high-performance III-V/Si triple-junction solar cells. A silver diffractive back reflector at the bottom of the cell is designed to steer incoming light to diffraction angles at which total internal refection occurs, in a wavelength range where light is poorly absorbed by Si. The performance dependence on the structural parameters is analyzed and explained with a simple interference model. Next, the impact of the optimized design on the absorption in a thick Si slab is evaluated, highlighting an increase over a planar back–reflector and over the design that is featured in the current world–record cell. Large area Si bottom cells and full two–terminal triple–junction cells are patterned via Substrate Conformal Imprint Lithography (SCIL) and characterized optically and electronically. The experimental external quantum efficiencies and one-sun current-voltage characteristics demonstrate a significant performance

improvement over the planar reference for complete triple-junction solar cells and over the current record cell design for the single-junction Si cells. These results highlight the potential to achieve efficiencies above the current record cell. Moreover, similar strategies can be applied to other Si-based tandem cells where standard random texture is not viable.

Overall, this thesis provides new insights into the design and understanding of metasurfaces for optical processing at visible wavelengths, and presents novel experimental demonstrations that can be realistically applied in hybrid optical–electronic devices opening new exciting opportunities for computing at high speed, low power, and small dimensions.

REFERENCES

[1] D. Psaltis and R. A. Athale, *High accuracy computation with linear analog optical systems: a critical study,* Applied Optics **25**, 3071 (1986).

[2] L. J. Cutrona, E. N. Leith, L. J. Porcello, and W. E. Vivian, *On the Application of Coherent Optical Processing Techniques to Synthetic-Aperture Radar,* Proceedings of the IEEE **54**, 1026 (1966).

[3] R. Athale and D. Psaltis, *Optical Computing: Past and Future,* Optics and Photonics News **27**, 32 (2016).

[4] Y. S. Abu-Mostafa and D. Psaltis, *Optical Neural Computers,* Scientific American **256**, 88 (1987).

[5] J. D. Armitage and A. W. Lohmann, *Character recognition by incoherent spatial filtering,* Applied Optics **4**, 461 (1965).

[6] H. J. Caulfield and W. T. Maloney, *Improved discrimination in optical character recognition,* Applied Optics **8**, 2354 (1969).

[7] D. L. Flannery and J. L. Horner, *Fourier optical signal processors,* Proceedings of the IEEE **77**, 1511 (1989).

[8] A. Lugt, *Coherent optical processing,* Proceedings of the IEEE **62**, 1300 (1974).

[9] H. Y. S. Li, Y. Qiao, and D. Psaltis, *Optical Network For Real-time Face Recognition,* Applied Optics **32**, 5026 (1993).

[10] J. W. Goodman, *Introduction to Fourier Optics*, 4th ed. (W. H. Freeman, 2017).

[11] A. Silva, F. Monticone, G. Castaldi, V. Galdi, A. Alu, and N. Engheta, *Performing Mathematical Operations with Metamaterials,* Science **343**, 160 (2014).

[12] A. Pors, M. G. Nielsen, and S. I. Bozhevolnyi, *Analog computing using reflective plasmonic metasurfaces,* Nano Letters **15**, 791 (2015).

[13] D. R. Solli and B. Jalali, *Analog optical computing,* Nature Photonics **9**, 704 (2015).

[14] T. Zhu, Y. Zhou, Y. Lou, H. Ye, M. Qiu, Z. Ruan, and S. Fan, *Plasmonic computing of spatial differentiation,* Nature Communications **8**, 15391 (2017).

[15] H. Kwon, D. Sounas, A. Cordaro, A. Polman, and A. Alù, *Nonlocal Metasurfaces for Optical Signal Processing,* Physical Review Letters **121**, 173004 (2018).

[16] A. Roberts, D. E. Gómez, and T. J. Davis, *Optical image processing with metasurface dark modes,* Journal of the Optical Society of America A **35**, 1575 (2018).

[17] C. Guo, M. Xiao, M. Minkov, Y. Shi, and S. Fan, *Isotropic wavevector domain image filters by a photonic crystal slab device,* Journal of the Optical Society of America A **35**, 1685 (2018).

[18] C. Guo, M. Xiao, M. Minkov, Y. Shi, and S. Fan, *Photonic crystal slab Laplace operator for image differentiation,* Optica **5**, 251 (2018).

[19] A. Cordaro, H. Kwon, D. Sounas, A. F. Koenderink, A. Alù, and A. Polman, *High-index dielectric metasurfaces performing mathematical operations,* Nano Letters **19**, 8418 (2019).

[20] S. A. Maier, *Plasmonics: Fundamentals and Applications*, 1st ed. (Springer US, New York, NY, 2007).

[21] F. Zangeneh-Nejad, D. L. Sounas, A. Alù, and R. Fleury, *Analogue computing with metamaterials,* Nature Reviews Materials **6**, 207 (2021).

[22] S. Abdollahramezani, O. Hemmatyar, and A. Adibi, *Meta-optics for spatial optical analog computing,* Nanophotonics **9**, 4075 (2020).

[23] L. Wesemann, T. J. Davis, and A. Roberts, *Meta-optical and thin film devices for all-optical information processing,* Applied Physics Reviews **8**, 031309 (2021).

[24] A. Youssefi, F. Zangeneh-Nejad, S. Abdollahramezani, and A. Khavasi, *Analog computing by brewster effect,* Opt. Lett. **41**, 3467 (2016).

[25] T. Zhu, Y. Lou, Y. Zhou, J. Zhang, J. Huang, Y. Li, H. Luo, S. Wen, S. Zhu, Q. Gong, M. Qiu, and Z. Ruan, *Generalized Spatial Differentiation from the Spin Hall Effect of Light and Its Application in Image Processing of Edge Detection,* Physical Review Applied **11**, 034043 (2019).

[26] T. Zhu, J. Huang, and Z. Ruan, *Optical phase mining by adjustable spatial differentiator,* Advanced Photonics **2**, 1 (2020).

[27] S. He, J. Zhou, S. Chen, W. Shu, H. Luo, and S. Wen, *Wavelength-independent optical fully differential operation based on the spin–orbit interaction of light,* APL Photonics **5**, 036105 (2020).

[28] T. Zhu, C. Guo, J. Huang, H. Wang, M. Orenstein, Z. Ruan, and S. Fan, *Topological optical differentiator,* Nature Communications **12**, 680 (2021).

[29] Y. Zhou, H. Zheng, I. I. Kravchenko, and J. Valentine, *Flat optics for image differentiation,* Nature Photonics **14**, 316 (2020).

[30] C. Guo, H. Wang, and S. Fan, *Squeeze free space with nonlocal flat optics,* Optica **7**, 1133 (2020).

[31] O. Reshef, M. P. DelMastro, K. K. M. Bearne, A. H. Alhulaymi, L. Giner, R. W. Boyd, and J. S. Lundeen, *An optic to replace space and its application towards ultra-thin imaging systems,* Nature Communications **12**, 3512 (2021).

[32] C. M. Lalau-Keraly, S. Bhargava, O. D. Miller, and E. Yablonovitch, *Adjoint shape optimization applied to electromagnetic design,* Optics Express **21**, 21693 (2013).

[33] A. Y. Piggott, J. Lu, K. G. Lagoudakis, J. Petykiewicz, T. M. Babinec, and J. Vucković, *Inverse design and demonstration of a compact and broadband on-chip wavelength demultiplexer,* Nature Photonics **9**, 374 (2015).

[34] D. Sell, J. Yang, S. Doshay, R. Yang, and J. A. Fan, *Large-Angle, Multifunctional Metagratings Based on Freeform Multimode Geometries,* Nano Letters **17**, 3752 (2017).

[35] A. Y. Piggott, J. Petykiewicz, L. Su, and J. Vučković, *Fabrication-constrained nanophotonic inverse design,* Scientific Reports **7**, 1786 (2017).

[36] T. W. Hughes, M. Minkov, I. A. D. Williamson, and S. Fan, *Adjoint Method and Inverse Design for Nonlinear Nanophotonic Devices,* ACS Photonics **5**, 4781 (2018), 1811.01255 .

[37] S. Molesky, Z. Lin, A. Y. Piggott, W. Jin, J. Vucković, and A. W. Rodriguez, *Inverse design in nanophotonics,* Nature Photonics **12**, 659 (2018).

[38] N. Mohammadi Estakhri, B. Edwards, and N. Engheta, *Inverse-designed metastructures that solve equations,* Science **363**, 1333 (2019).

[39] M. Camacho, B. Edwards, and N. Engheta, *A single inverse-designed photonic structure that performs parallel computing,* Nature Communications **12**, 1466 (2021).